NACA

RESEARCH MEMORANDUM

ADDITIONAL MEASUREMENTS OF THE LOW-SPEED STATIC

STABILITY OF A CONFIGURATION EMPLOYING

THREE TRIANGULAR WING PANELS

AND A BODY OF EQUAL LENGTH

By Noel K. Delany

Ames Aeronautical Laboratory
Moffett Field, Calif.

This material contains information affecting the National Defense of the United States within the meaning of the espionage laws, Title 18, U.S.C., Secs. 793 and 794, the transmission or revelation of which in any manner to an unauthorized person is prohibited by law.

NATIONAL ADVISORY COMMITTEE
FOR AERONAUTICS

WASHINGTON
July 25, 1955

NATIONAL ADVISORY COMMITTEE FOR AERONAUTICS

RESEARCH MEMORANDUM

ADDITIONAL MEASUREMENTS OF THE LOW-SPEED STATIC

STABILITY OF A CONFIGURATION EMPLOYING

THREE TRIANGULAR WING PANELS

AND A BODY OF EQUAL LENGTH

By Noel K. Delany

SUMMARY

An experimental investigation has been conducted at low speeds of
the static-stability characteristics of a simplified model of an unusual
configuration. The model had three triangular airfoils of low aspect
ratio. One of the airfoils was mounted vertically on top of a body of
revolution as a fin, and the other two were mounted as the main lifting
surfaces. The leading edges of the airfoils used as the main lifting
surfaces were swept back 73.9^O. Two vertical fins were investigated;
one was the same as the main lifting surfaces, the other had the leading
edge swept back 76.0^O. The body had the same length as the airfoils.

Results of tests of the simplified model of the configuration are
presented for a large range of angles of attack and sideslip for several
dihedral angles. Some data were also obtained on the damping-in-roll
characteristics of the model at 0° angles of attack and sideslip.

INTRODUCTION

An airplane configuration having three identical triangular airfoils
of low aspect ratio radiating symmetrically from a central body that does
not protrude ahead of the wings has been suggested as a promising arrange-
ment for flight at very high speeds. The results of an investigation of
the low-speed static stability of a simplified model of such an arrange-
ment having one of the airfoils placed vertically on top of the body and
the other two as wing panels having negative dihedral are presented in
reference 1.

In order to provide information for predicting the effects of changes in the basic configuration on the low-speed stability characteristics presented in reference 1, additional measurements have been made. The effects of changes in dihedral and in the size of the vertical fin were investigated for a large range of angles of attack and sideslip. The contributions of the various components of the model to the static stability and to the damping in roll were also considered.

The investigation was conducted in a 7- by 10-foot wind tunnel at the Ames Aeronautical Laboratory at a Mach number of approximately 0.25 which corresponded to a Reynolds number of about 4.5 million based on the mean aerodynamic chord.

NOTATION

A diagram showing the system of axes and the positive directions of forces and moments used in presenting the data is shown in figure 1. The axes of all forces and moments pass through the moment center of the model. The moment center was 0.37 of the mean aerodynamic chord behind the leading edge of the mean aerodynamic chord. Both the body axes and the stability system of axes are defined in figure 1; however, unless otherwise specified all results are presented with respect to the body axes. The symbols used in the report are defined as follows:

b wing span (twice the panel span), ft

$\bar{c}$ mean aerodynamic chord of the wing, $\dfrac{\displaystyle\int_0^{b/2} c^2\,dy}{\displaystyle\int_0^{b/2} c\,dy}$, ft

c wing chord parallel to plane of symmetry, ft

C_A axial-force coefficient, $\dfrac{F_A}{qS}$

C_{D_s} drag coefficient referred to stability axes, $\dfrac{F_{D_s}}{qSb}$

C_L lift coefficient, $\dfrac{F_L}{qS}$

C_l rolling-moment coefficient referred to body axes, $\dfrac{M_X}{qSb}$

C_{l_p} rate of change of rolling-moment coefficient with rolling-angular-velocity factor $\dfrac{\partial C_{l_s}}{\partial (pb/2V_o)}$

C_{l_s} rolling-moment coefficient referred to stability axes, $\dfrac{M_{X_s}}{qSb}$

C_m pitching-moment coefficient, $\dfrac{M_Y}{qS\bar{c}}$

C_N normal-force coefficient, $\dfrac{F_N}{qS}$

C_n yawing-moment coefficient referred to body axes, $\dfrac{M_Z}{qSb}$

C_{n_s} yawing-moment coefficient referred to stability axes, $\dfrac{M_{Z_s}}{qSb}$

C_Y side-force coefficient, $\dfrac{F_Y}{qS}$

F_A axial force, positive along $-X$ axis, lb

F_{D_s} drag force, positive along $-X_s$ axis, lb

F_L lift force, positive along $-Z_s$ axis, lb

F_N normal force, positive along $-Z$ axis, lb

F_Y side force, positive along the Y or Y_s axis, lb

$\dfrac{L}{D}$ ratio of lift to drag $\dfrac{C_L}{C_{D_s}}$

M_X rolling moment about the X axis, positive clockwise looking forward, ft-lb

M_{X_s} rolling moment about the X_s axis, positive clockwise looking forward, ft-lb

M_Y pitching moment about the Y or Y_s axis, positive moment raises the nose, ft-lb

M_Z yawing moment about Z axis, positive moment rotates nose to right, ft-lb

M_{Z_s} yawing moment about Z_s axis, positive moment rotates nose to right, ft-lb

p rolling angular velocity, radians per/sec

$\dfrac{pb}{2V_o}$ rolling-angular-velocity factor of helix generated by wing tip in roll, radians

q dynamic pressure, lb/sq ft

S wing area (twice panel area), sq ft

V_o free-stream velocity, ft/sec

α   angle of attack, deg

β   angle of sideslip, deg

Γ   dihedral angle, deg

δ_a total aileron deflection, positive deflection gives a positive
             rolling moment, deg

δ_r rudder deflection, positive, trailing edge to left, deg

X   longitudinal body axis, in vertical plane of symmetry and
             coincident with center line of body, positive forward

X_s longitudinal stability axis, parallel to the projection of the
             relative wind on the vertical plane of symmetry, positive
             forward

Y   lateral body axis, perpendicular to vertical plane of symmetry,
             positive to right when looking forward

Y_s lateral-stability axis, perpendicular to vertical plane of
             symmetry, positive to right when looking forward

Z   vertical body axis, in vertical plane of symmetry and perpen-
             dicular to the longitudinal and lateral body axes, positive
             downward

Z_s vertical stability axis, in vertical plane of symmetry and
             perpendicular to the relative wind, positive downward

MODEL AND APPARATUS

        The model and apparatus were the same as those used in the investi-
gation reported in reference 1. The basic model consisted of three identi-
cal triangular airfoils radiating symmetrically from a body of revolution
as shown in figure 2. The wing surfaces were 3/4-inch Douglas fir plywood
with blunt trailing edges and with sharpened leading edges of solid mahog-
any. The wood was finished with a surface sealer, but a high degree of
smoothness was not attempted. The panels were attached to the body with
sheet-metal brackets inlaid flush into the airfoils but external to the
surface of the body so as to facilitate changing the angular relation of
the airfoils. It was possible to set the wing at dihedral angles of 0°,
-15°, and -30°.

        Two different size airfoils were tested as the vertical surface.
One had the same dimensions as the airfoils used for the wing, while the

other had the same root chord but a smaller span. The pertinent geometric
characteristics of the airfoils are tabulated below:

Wing panels and large vertical fin
Aspect ratio 0.58
Root chord, ft 3.96
Span, body center line to tip, ft 1.14
Area, sq ft 2.26
Mean aerodynamic chord, ft . . . . 2.64 .
Sweepback of leading edge, deg 73.9
Small vertical fin
Aspect ratio 0.50
Root chord, ft 3.96
Span, body center line to tip, ft 0.99
Mean aerodynamic chord, ft 2.64
Sweepback of leading edge, deg 76.0

A deflected rudder was simulated by a full-span (at the hinge line)
split flap made of sheet metal and attached to the vertical fin with
wedge-shaped brackets. The chord of the flap was 6 percent of the airfoil
root chord.

The model was supported on a sting-mounted, four-component, strain-
gage balance contained within the body. The diameter of the sting at the
base of the body was 3.1 inches. A static-pressure orifice was installed
in the annular space between the sting and the body to permit measurement
of the average base pressure.

TESTS AND REDUCTION OF DATA

The sting support permitted angular movement of the model only about
a vertical axis passing through the moment center; hence the angle of
attack and angle of sideslip could not be varied independently. With one
of the airfoils horizontal (considered the vertical fin), the angle of
attack was varied at 0° sideslip, and with the same airfoil vertical, the
angle of sideslip was varied at 0° angle of attack. Intermediate settings
of the angle of bank produced attitudes of the model which combined finite
angles of attack and sideslip. Data for specific angles of attack combined
with sideslip were obtained by cross-plotting the basic wind-tunnel data
for the model set to various intermediate angles of bank.

All forces and moments were measured relative to a system of orthogo-
nal axes that were fixed with respect to the model (body axes). For a
given attitude of the model in the wind tunnel, and with the four-component
strain-gage balance properly alined relative to the model, F_N, F_A, M_Y, and
M_X were measured. For the same attitude of the model in the wind tunnel
but with the balance rotated 90° about its longitudinal axis from the above

position, F_Y, F_A, M_Z, and M_X were measured. Hence, for conditions where three force and three moment components were desired, it was necessary to obtain data for both positions of the balance relative to the model.

The steady-rolling technique was used to evaluate the damping in roll due to rolling for angles of attack and sideslip of 0°. For these tests the model was free to roll about the body axis. The split flaps were used as aerodynamic controls to drive the model in roll, and an electronic timer was used to measure the rate of roll. Since the rate of roll varied slightly due to flow fluctuations of the wind-tunnel stream, average values over a period of approximately 1 minute were used. The effect of friction on the rate of roll was negligible for the conditions presented.

The average pressure at the base of the model was measured, and the drag data have been corrected to correspond to a base pressure equal to free-stream static pressure. Because of the uncertainty of tunnel constriction effects and the exploratory nature of the investigation, no tunnel-wall corrections have been applied to the results.

RESULTS AND DISCUSSION

The results presented in reference 1 mainly pertain to the configuration with a dihedral angle of -30°. Measurements have been made with the same model as that of reference 1 to show the effects of the various components of the model on the static aerodynamic characteristics for several dihedral angles. Also included in the present report are some measurements of the static-stability characteristics with a smaller vertical tail, and of the damping in roll due to rolling.

The lift coefficient, pitching-moment coefficient, and lift-drag ratio of the body alone and of the wing-body combinations for dihedral angles of 0°, -15°, and -30° are presented in figure 3 for a large range of angles of attack. It is noted that for a given angle of attack, less than about 24°, the lift coefficient varied with dihedral angle approximately as the square of the cosine of the dihedral angle.

The effects of the various components of the model (body alone, body plus large vertical fin, body plus wings, and complete model) on the variations with angle of sideslip of yawing-moment, rolling-moment, and side-force coefficients for an angle of attack of 0° are shown in figures 4(a), (b), and (c) for dihedral angles of 0°, -15°, and -30°, respectively. In general, these variations of the lateral- and directional-stability coefficients with sideslip angle were approximately linear to 20° and did not have any sharp changes to 32°. Comparison of the data in figure 4 indicates that the mutual interference of the wing and the tail, for angles of sideslip of 0° to 16°, made C_{n_β} and C_{l_β} more positive and C_{Y_β} more

negative. The effect of the dihedral angle on the increment of C_{n_β} and C_{l_β} due to the interference was negligible; however, the increment of C_{Y_β} due to the interference became more negative as the dihedral angle became more negative.

The effect of angle of attack on the forces and moments due to the split-flap control on the vertical fin (rudder) is shown in figure 5 for the model with -30° of dihedral. For angles of attack between -8° and 32° the values of $C_{n_{\delta_r}}$ and $C_{l_{\delta_r}}$ remained approximately constant at -0.0014 and 0.0004, per degree, respectively. For the same type and size of control on the wing, values of $C_{n_{\delta_a}}$ and $C_{l_{\delta_a}}$ of 0.0007 and 0.0005, respectively (data not shown), were measured at 0° angle of attack (δ_a is considered to be the total aileron deflection). From these values it can be noted that piloting procedure for a coordinated turn would differ from that for a conventional airplane because of the rather large adverse rolling moment due to rudder deflection and the favorable yawing moment due to aileron deflection.

The variation with angle of sideslip of yawing-moment, rolling-moment, side-force, normal-force, pitching-moment, and axial-force coefficients are presented in figures 6 and 7 for various angles of attack from 0° to 40°. The data in figure 6 are for the model with -15° of dihedral and the large vertical fin; while the data in figure 7 are for the model with 0° of dihedral and the small vertical fin. The changes of these coefficients with angle of sideslip were relatively linear for angles of attack and sideslip up to about 20°. Figure 8 summarizes the effects of angle of attack on the static-stability parameters C_{n_β} and C_{l_β}. The variations of C_{n_β} and C_{l_β} were derived from the data in figure 6 of reference 1 and figures 6 and 7 of the present report for small angles of sideslip near zero. The variation with angle of attack of these parameters referred to the stability system of axes is also shown in figure 8. Interpolation between the data in figures 8(a) and (b) indicates that a model with a dihedral angle of approximately -25° and the large vertical fin would have the minimum variation with angle of attack of C_{n_β} and C_{l_β} referred to the stability axes. The interpolation also indicates that C_{n_β} and C_{l_β} for this configuration would be approximately 0.0015 and -0.0003, respectively, between angles of attack of 0° and 13°.

The measured damping-in-roll parameter, C_{l_p}, for 0° angle of attack and sideslip was 0.126 for two airfoils 180° apart ($\Gamma = 0^\circ$), and was 0.157 for three airfoils 120° apart ($\Gamma = -30^\circ$). Thus, three airfoils produced approximately 25 percent more damping than the two.
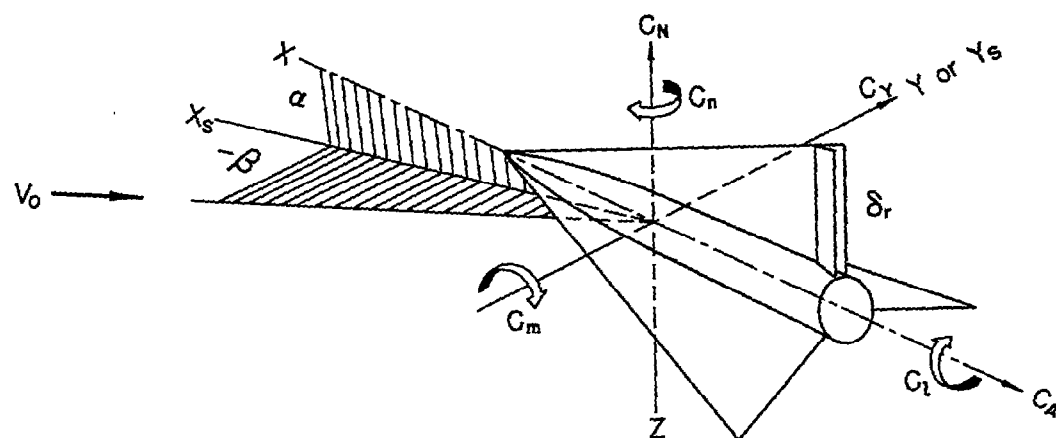
Ames Aeronautical Laboratory
    National Advisory Committee for Aeronautics
        Moffett Field, Calif., June 2, 1955
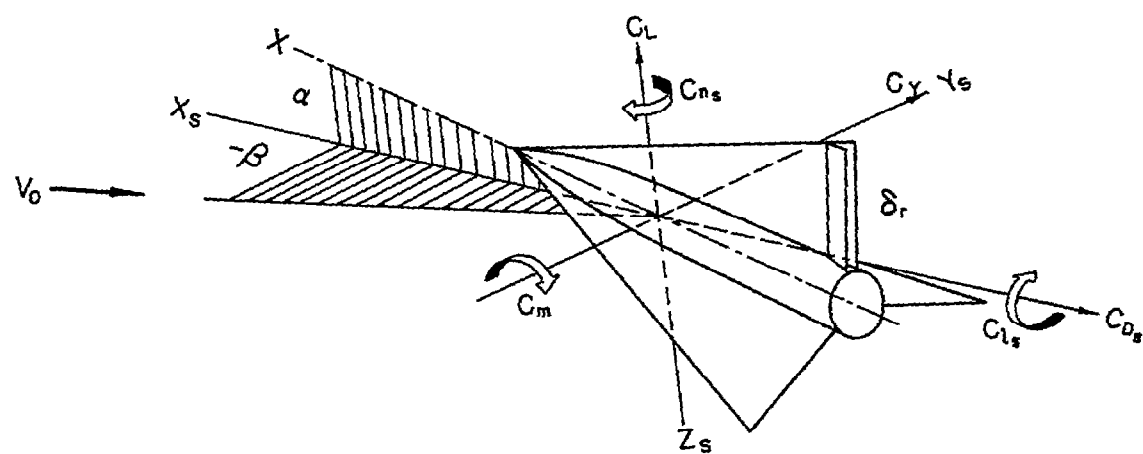
REFERENCE :

1. Delany, Noel K.: Exploratory Investigation of the Low-Speed Static
       Stability of a Configuration Employing Three Identical Triangular
       Wing Panels and a Body of Equal Length. NACA RM A55C28, 1955.

(a) Body axes.

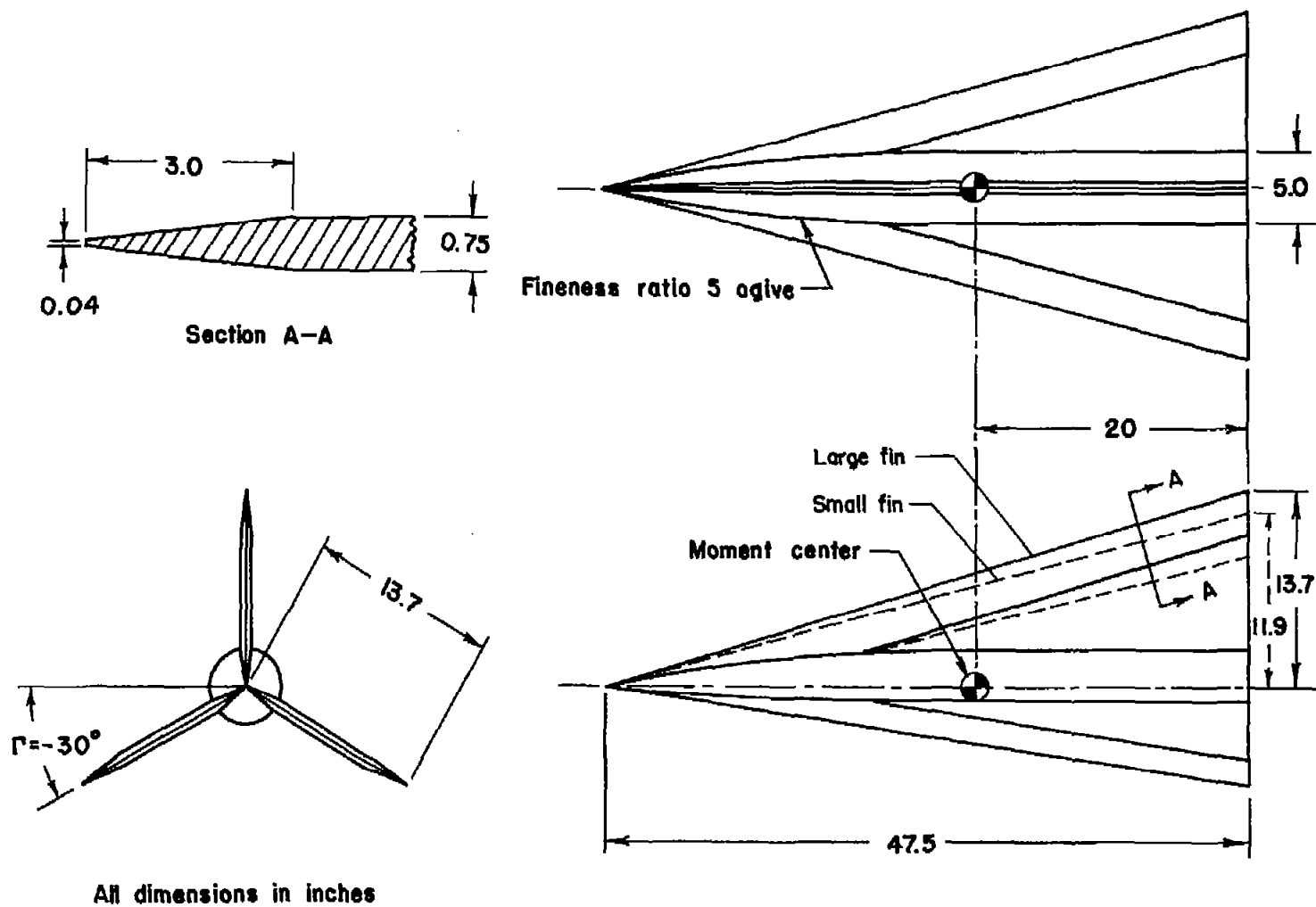(b) Stability axes.

Figure 1.- Systems of axes and sign convention.

3.0

0.75

0.04

Section A—A

Fineness ratio 5 ogive

5.0

20

Large fin

Small fin

Moment center

A

A

13.7

11.9

13.7

Γ=-30°

47.5

All dimensions in inches

Figure 2.- Sketch of the model.
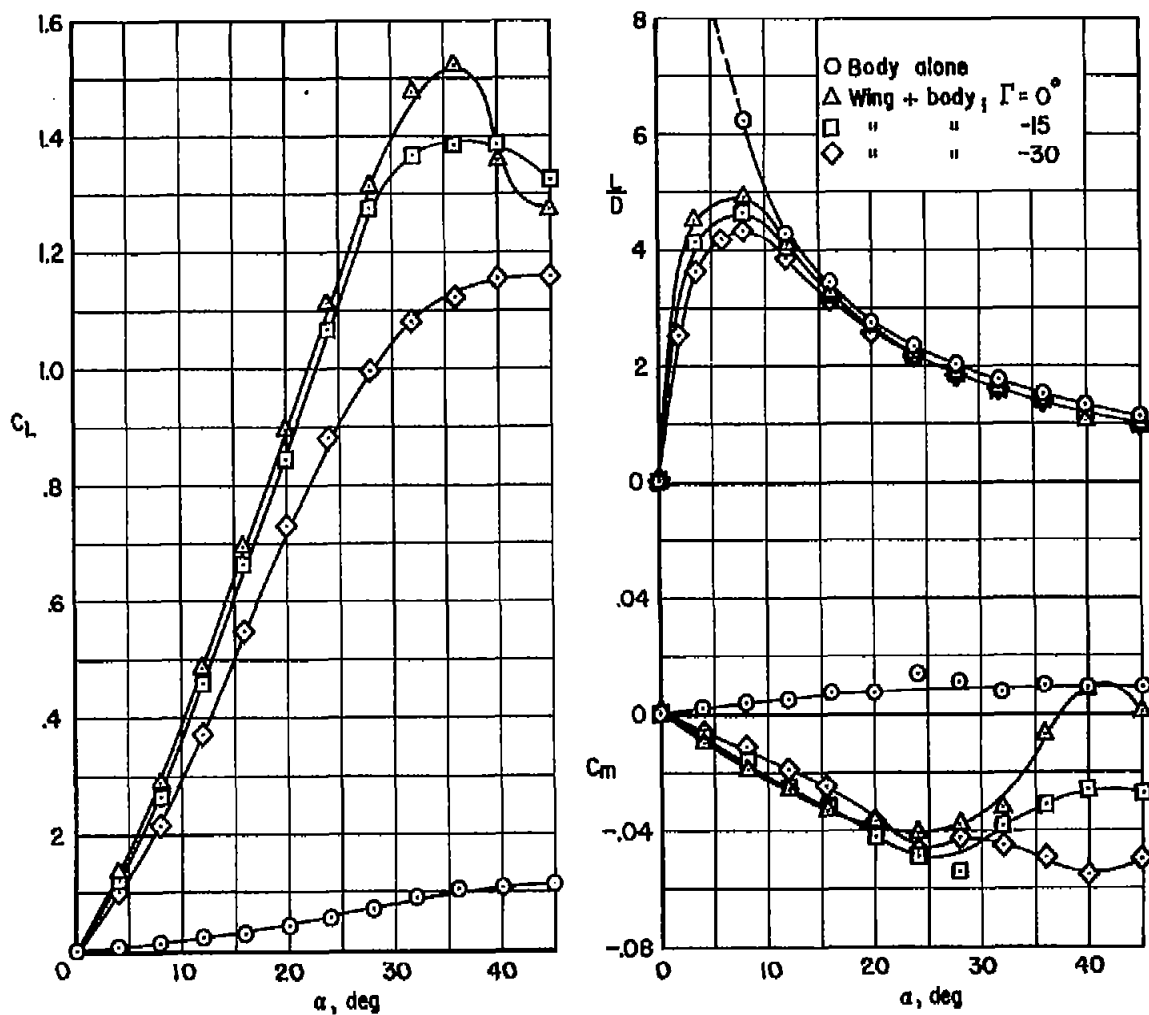
Figure 3.- Static longitudinal-stability characteristics for several dihedral angles; large vertical fin.

(a) $\Gamma = 0^{O}$.
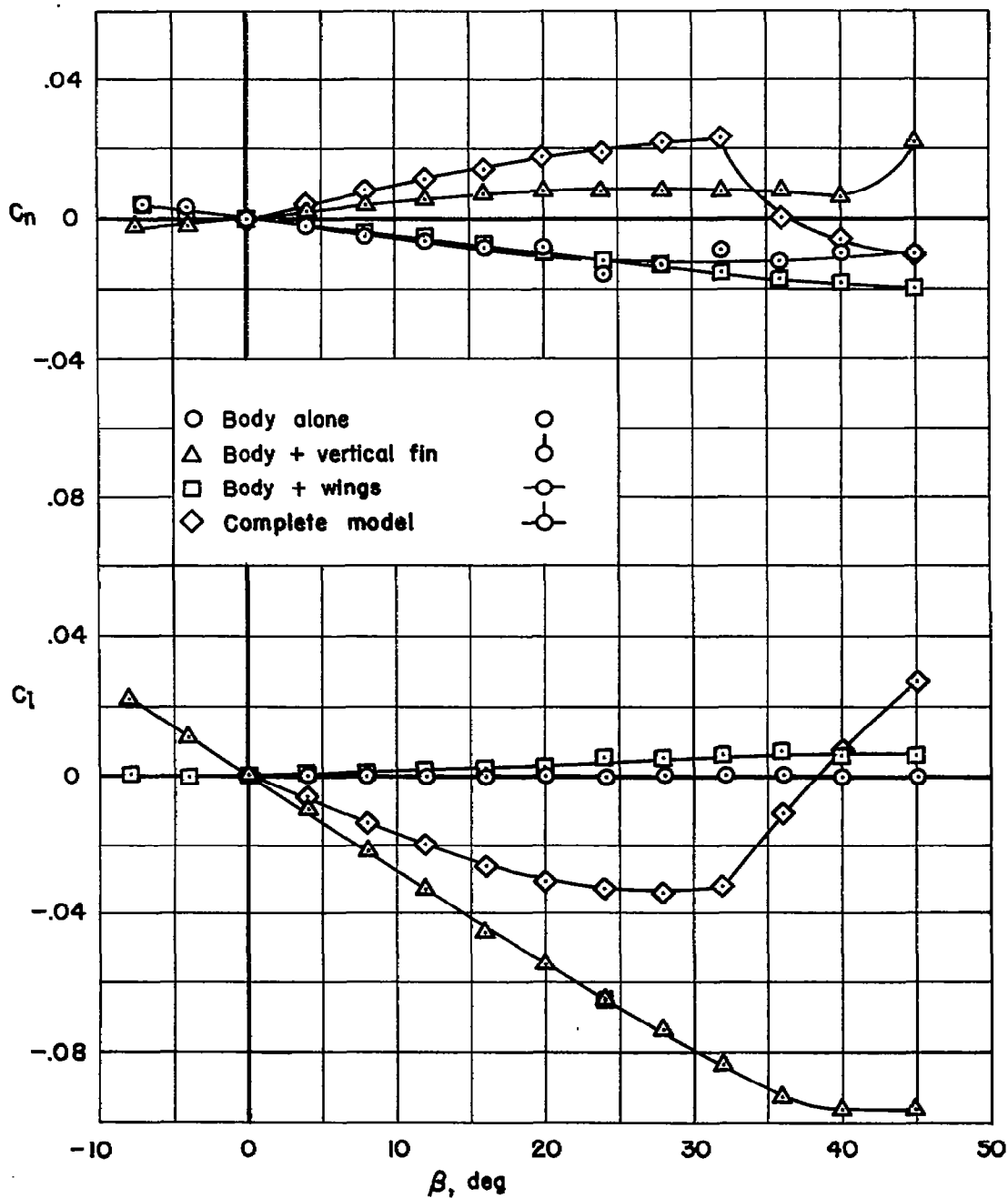
Figure 4.- Effect of the component parts of the model on the static
lateral and directional stability characteristics at $\alpha = 0^{O}$;
large vertical fin.
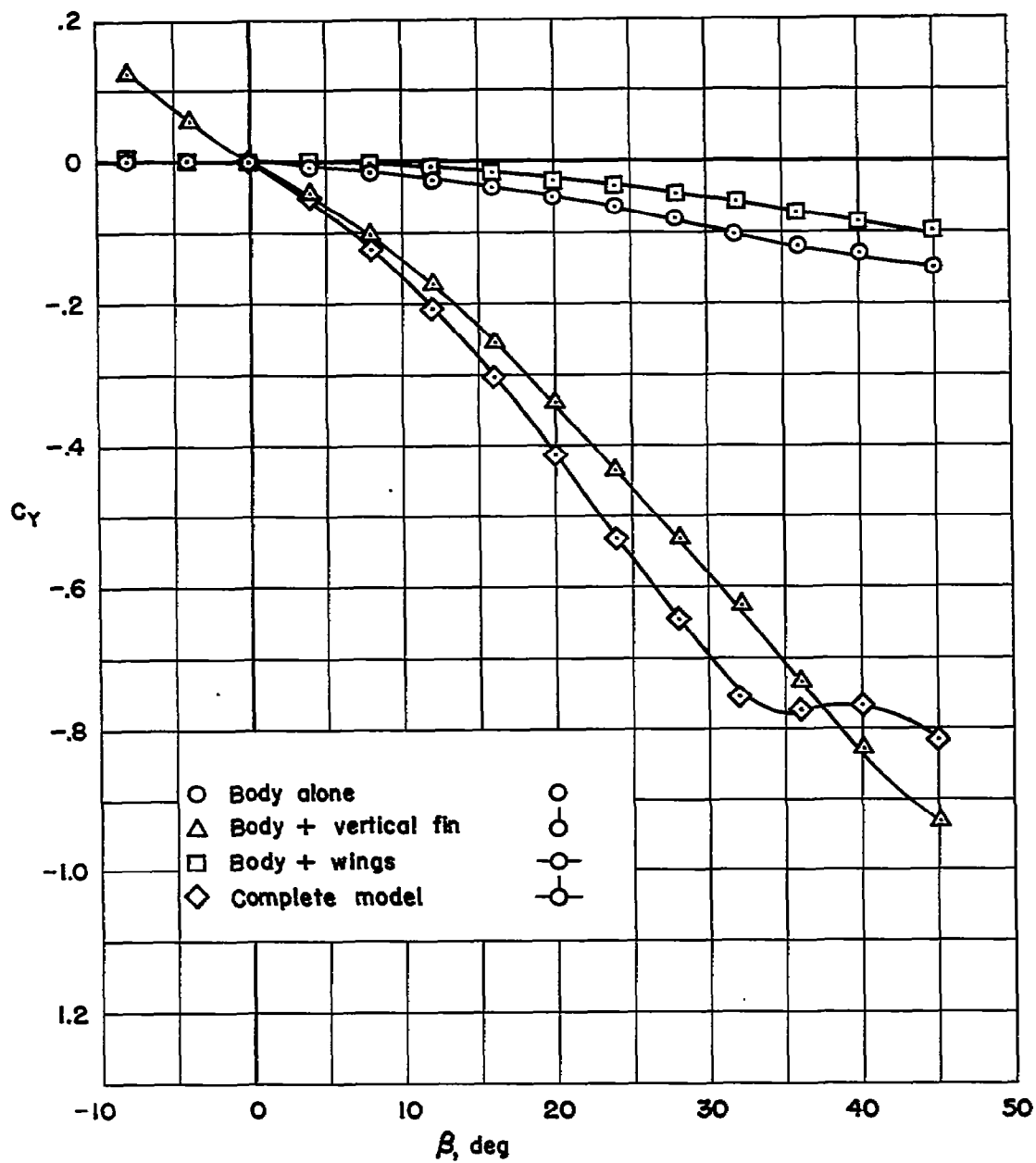
(a) Concluded.

Figure 4.- Continued.
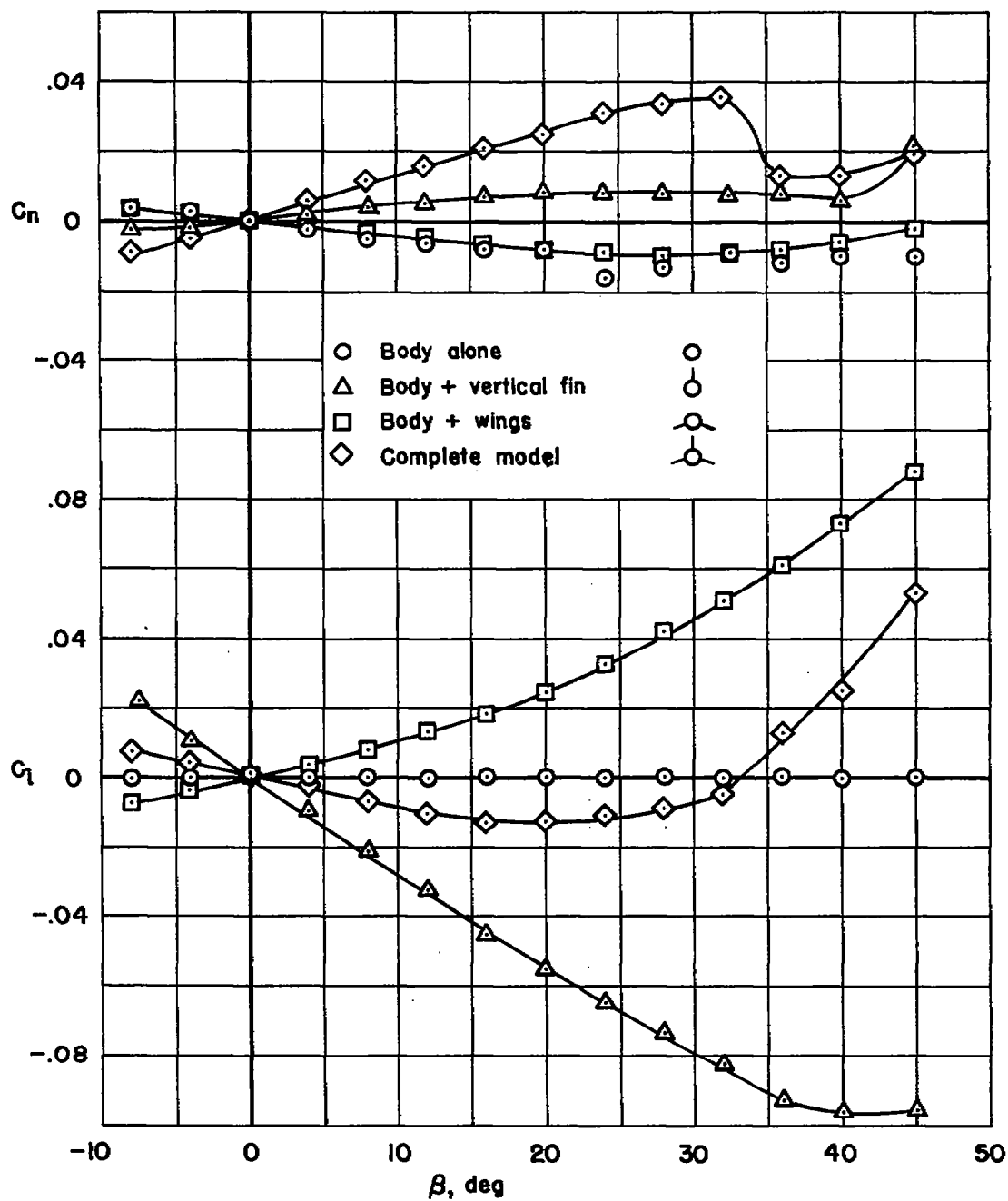
(b) $\Gamma = -15^\circ$.

Figure 4.- Continued.
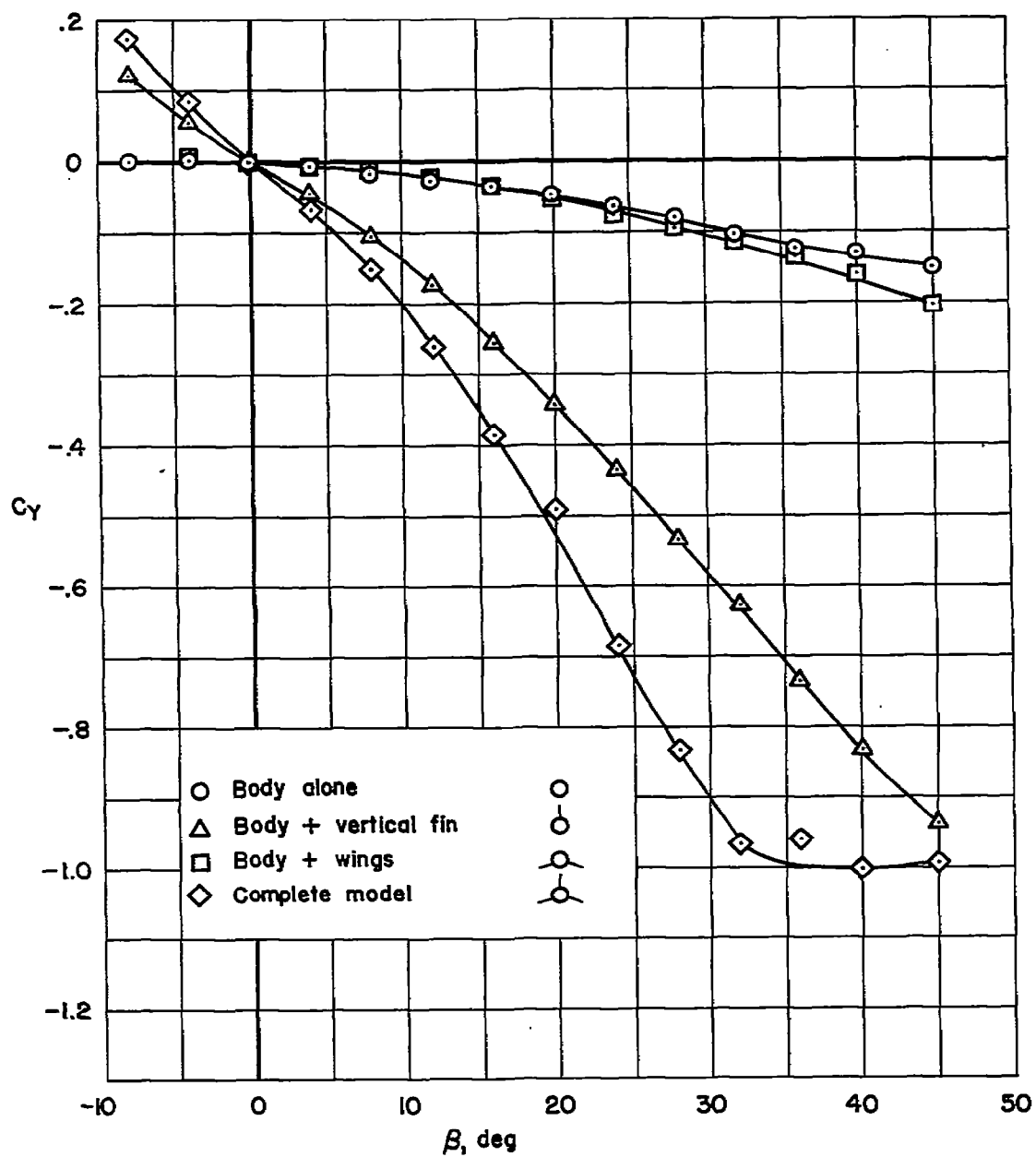
(b) Concluded.

Figure 4.- Continued.
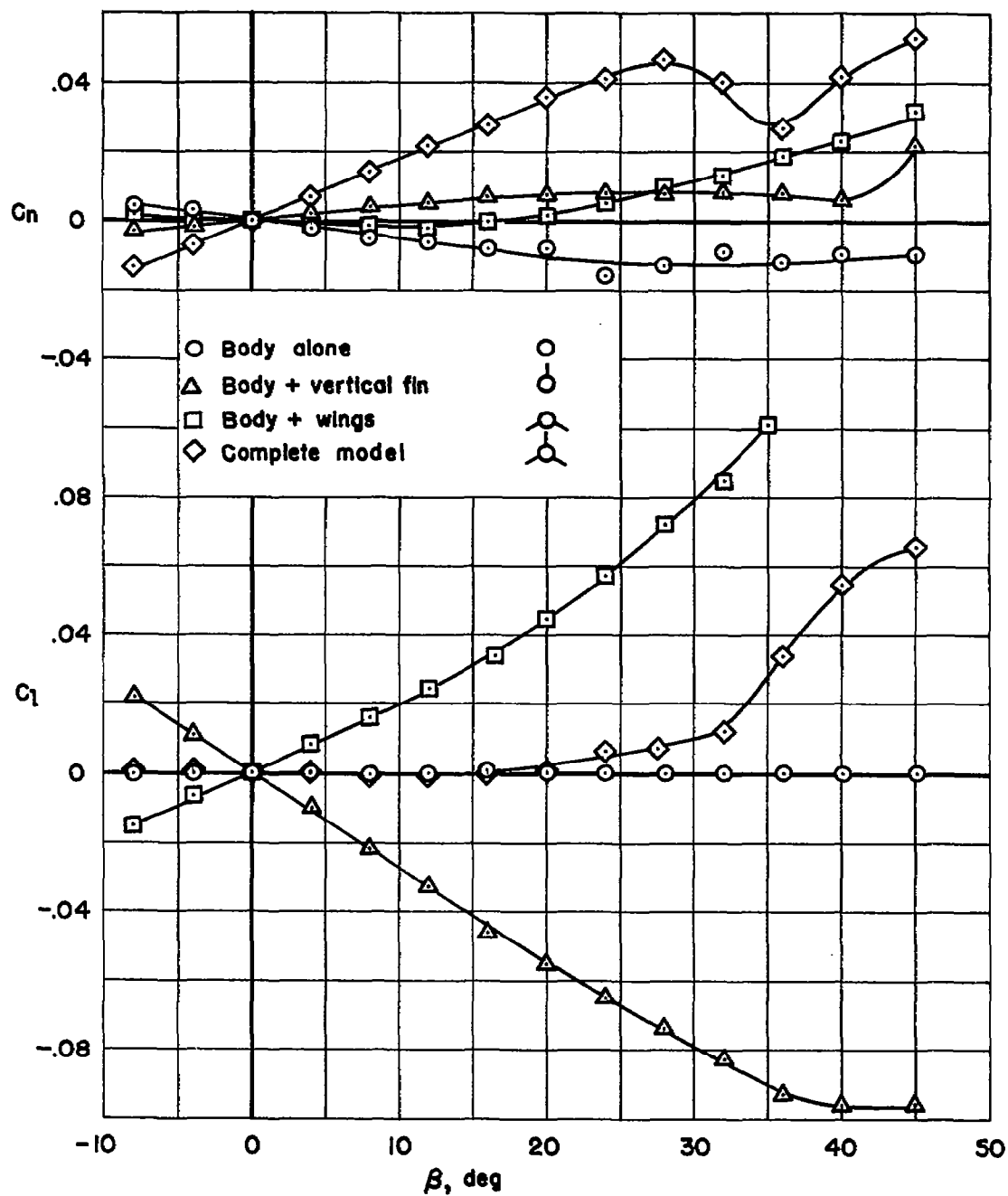
(c) $\Gamma = -30°$.

Figure 4.- Continued.
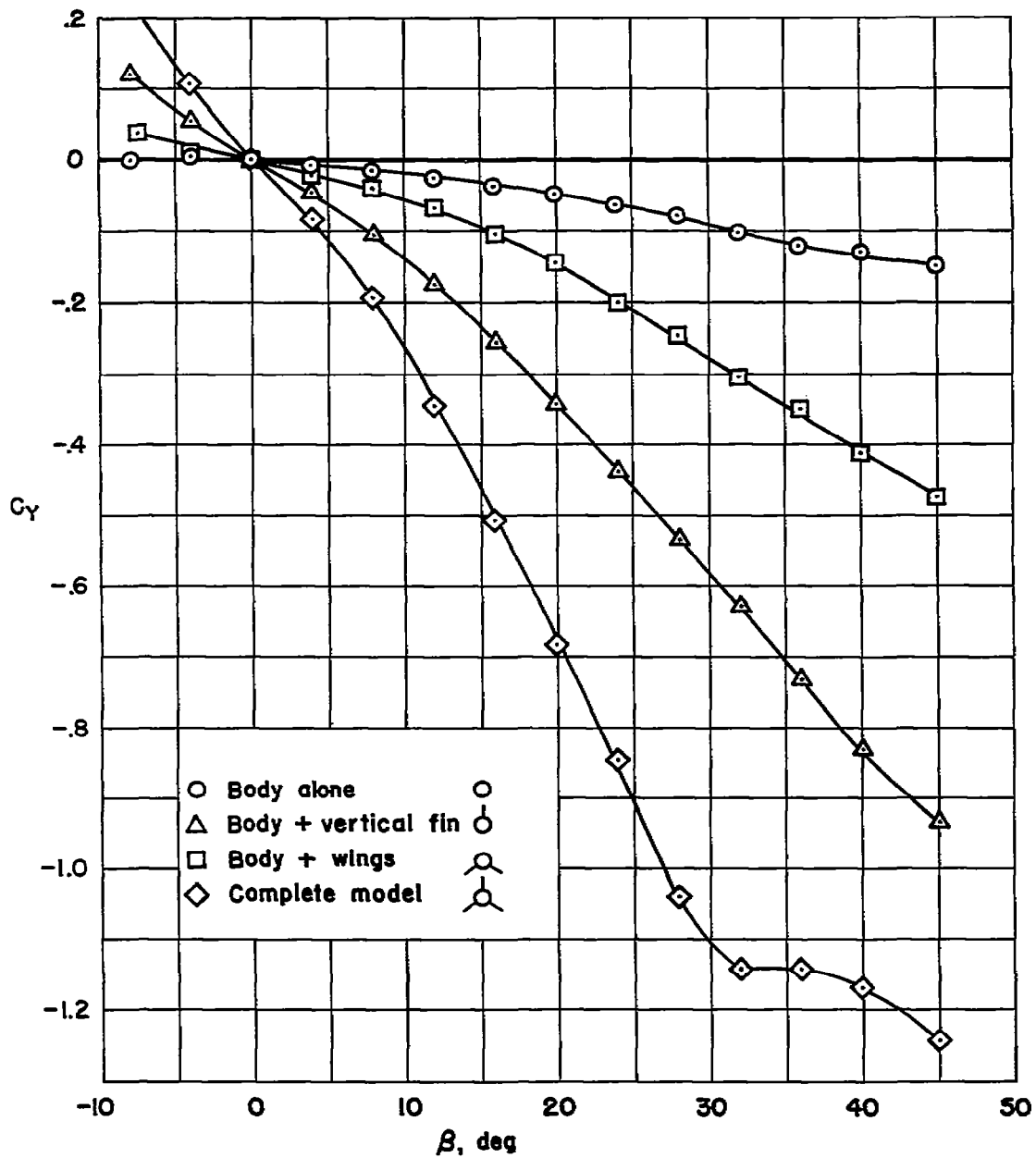
(c) Concluded.

Figure 4.- Concluded.
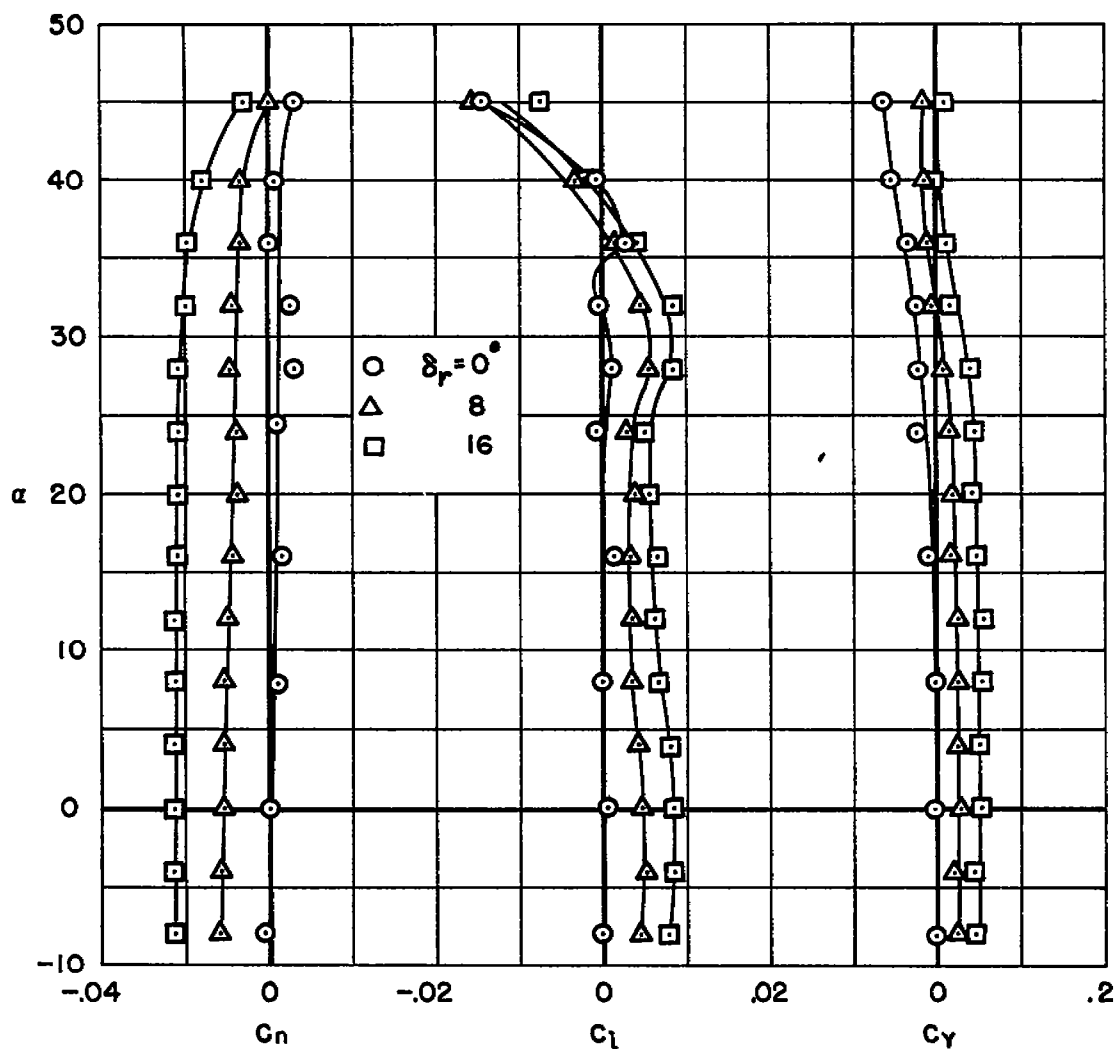
Figure 5.- The effect of angle of attack on the rudder effectiveness at zero sideslip; $\Gamma = -30°$, large vertical fin.
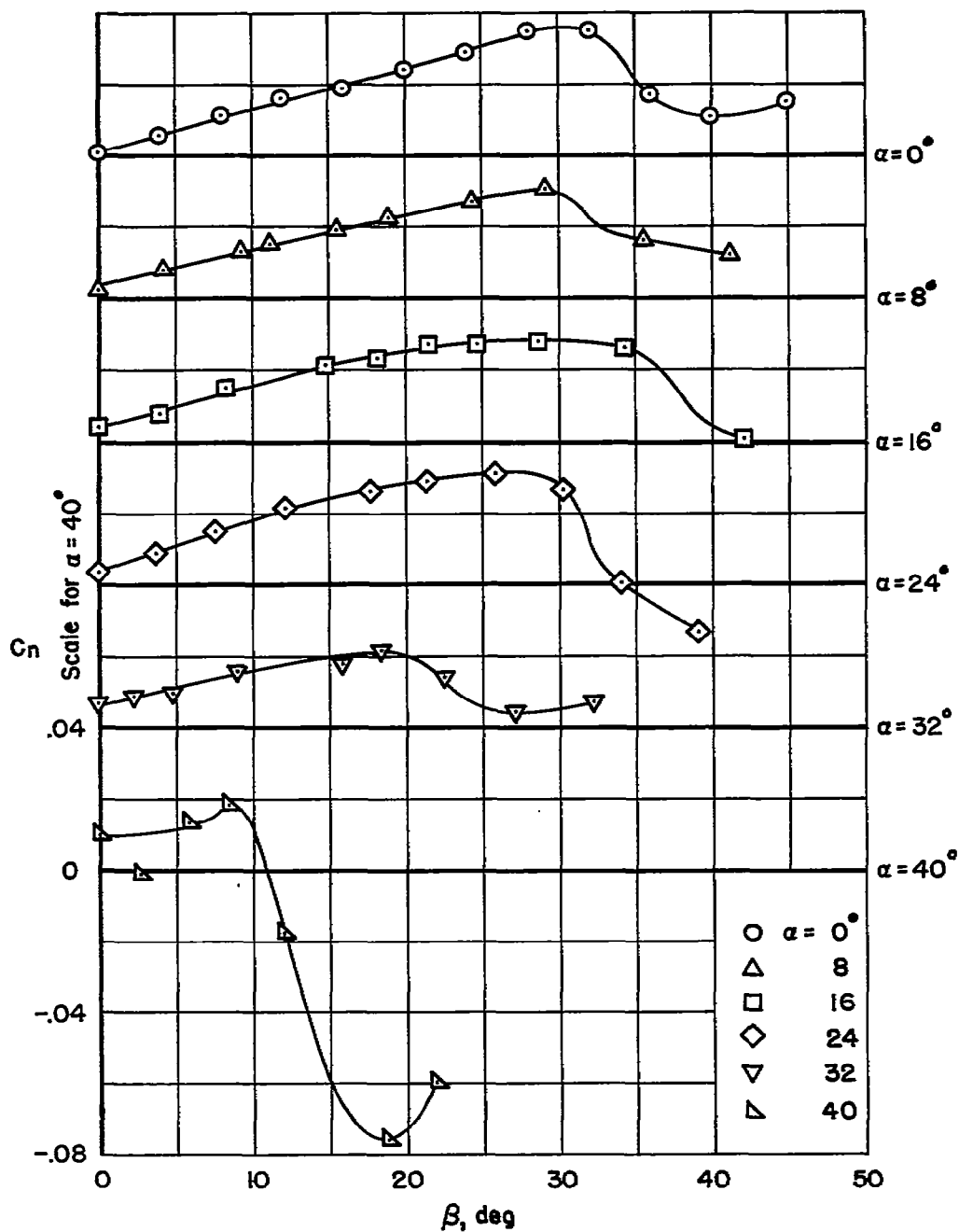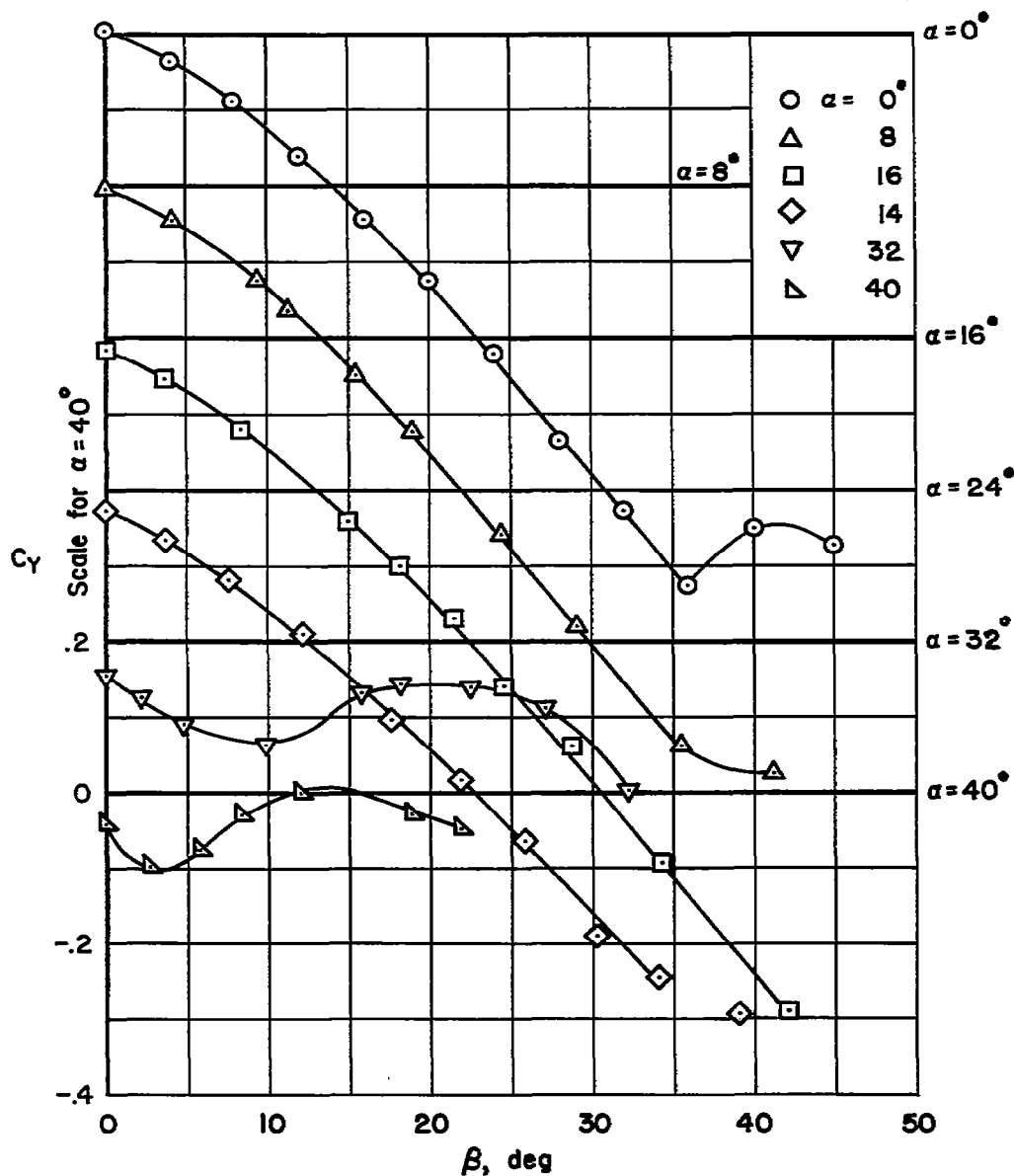
(a) Yawing-moment coefficient versus sideslip angle.

Figure 6.- Force and moment coefficients in sideslip for several angles
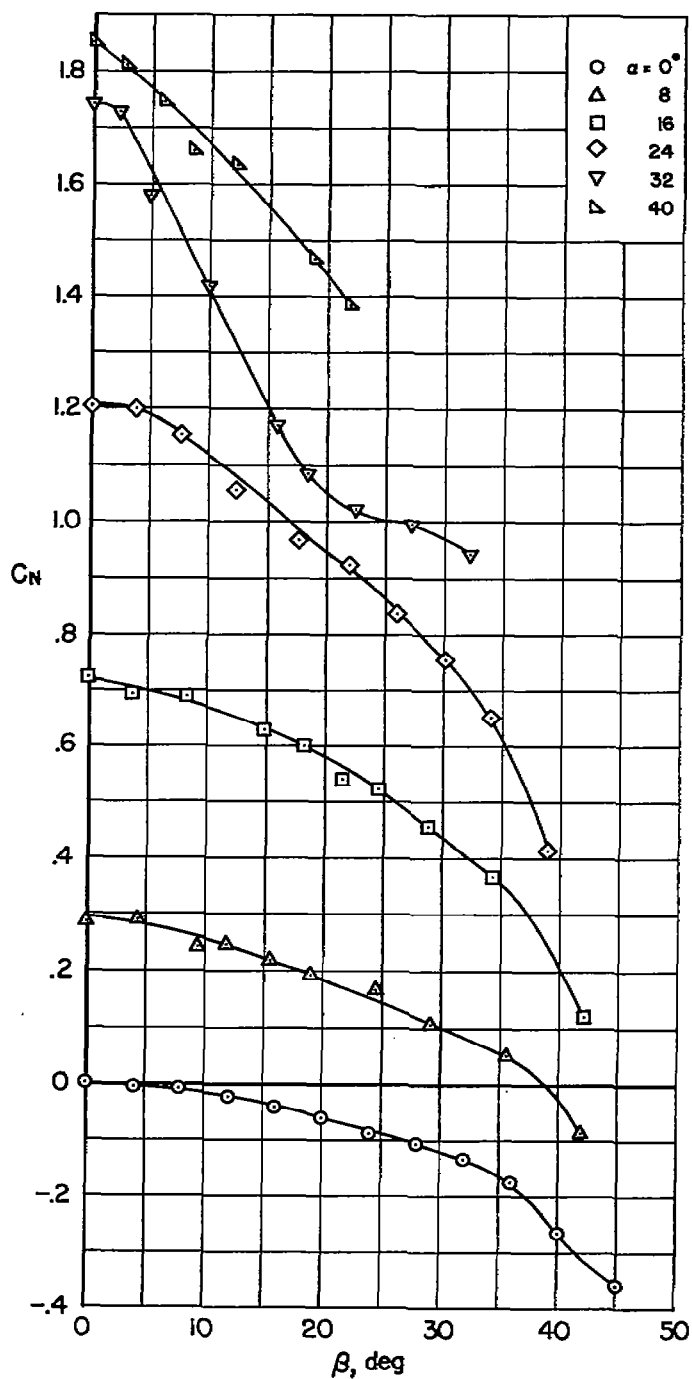of attack; $\Gamma = -15^{\circ}$, large vertical fin.
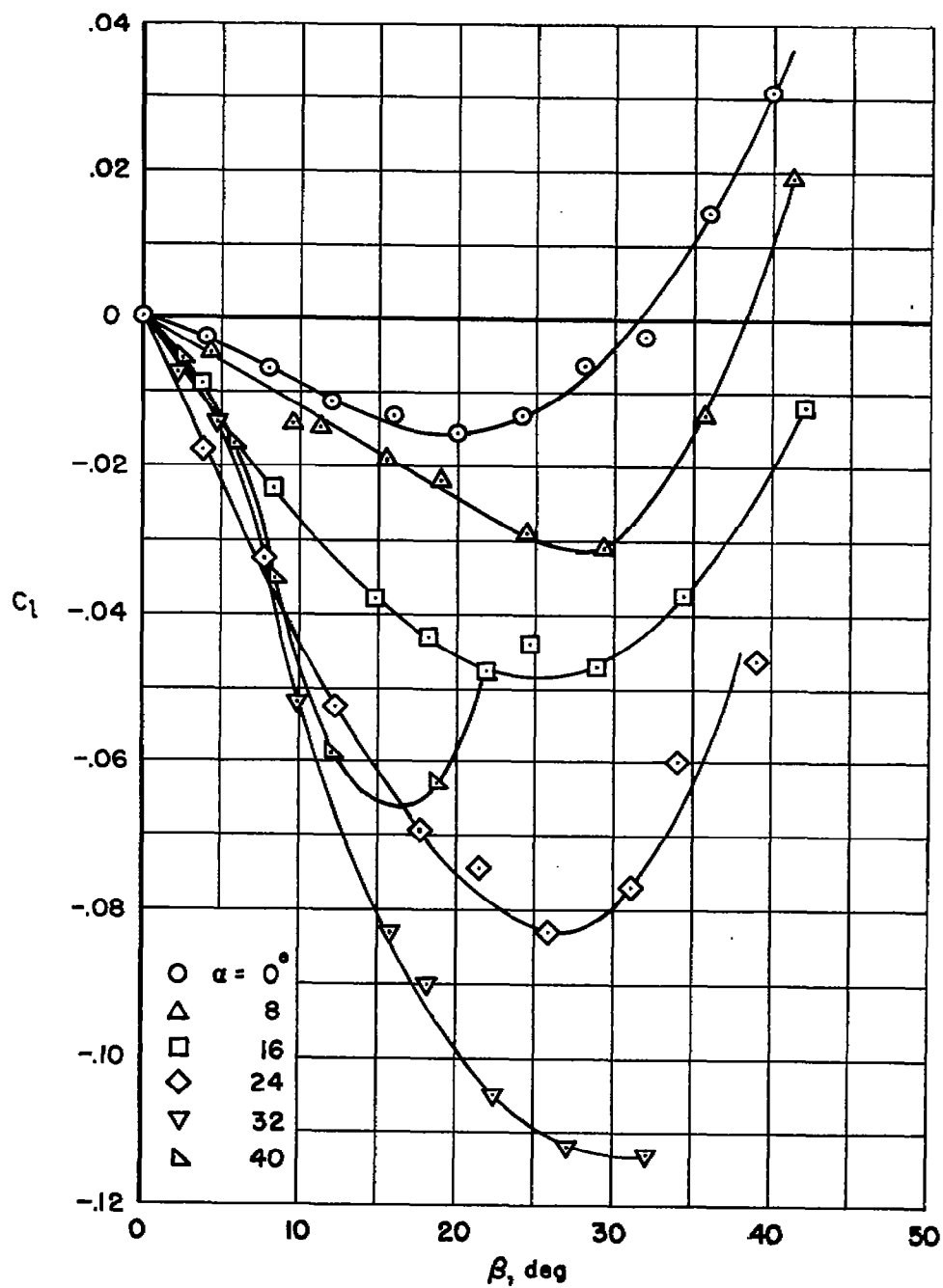
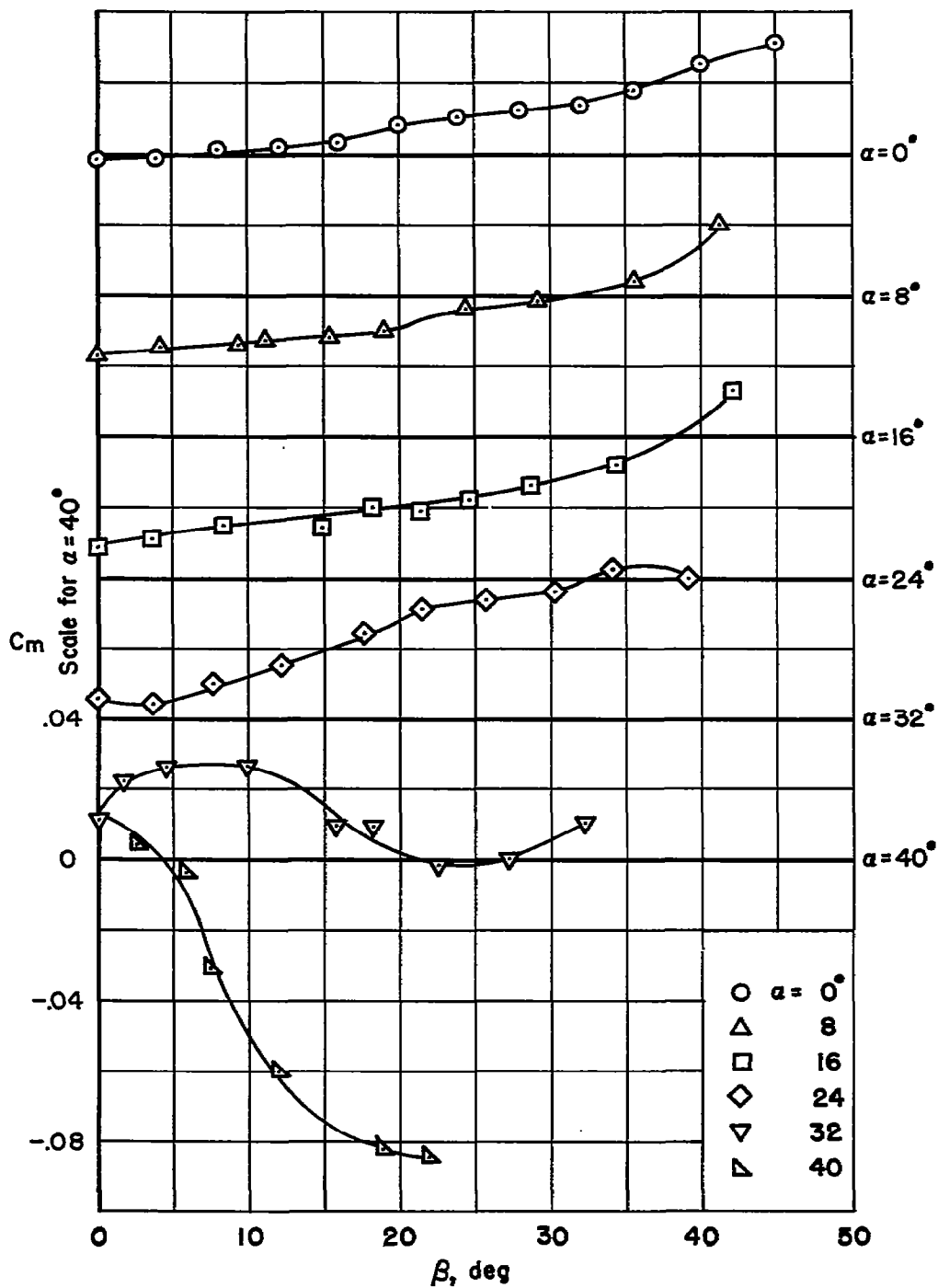(b) Rolling-moment coefficient versus sideslip angle.
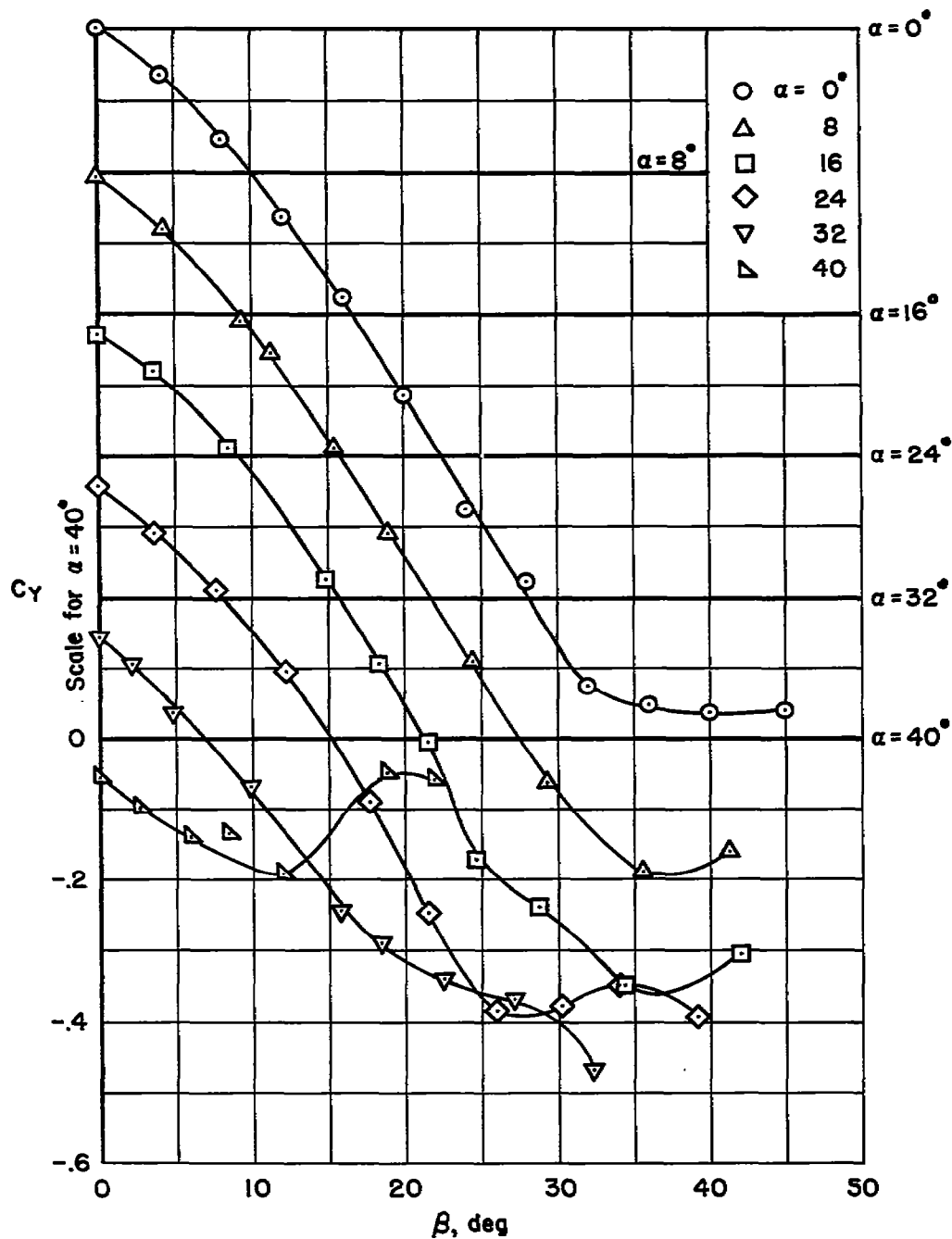
Figure 6.- Continued.

(c) Side-force coefficient versus sideslip angle.
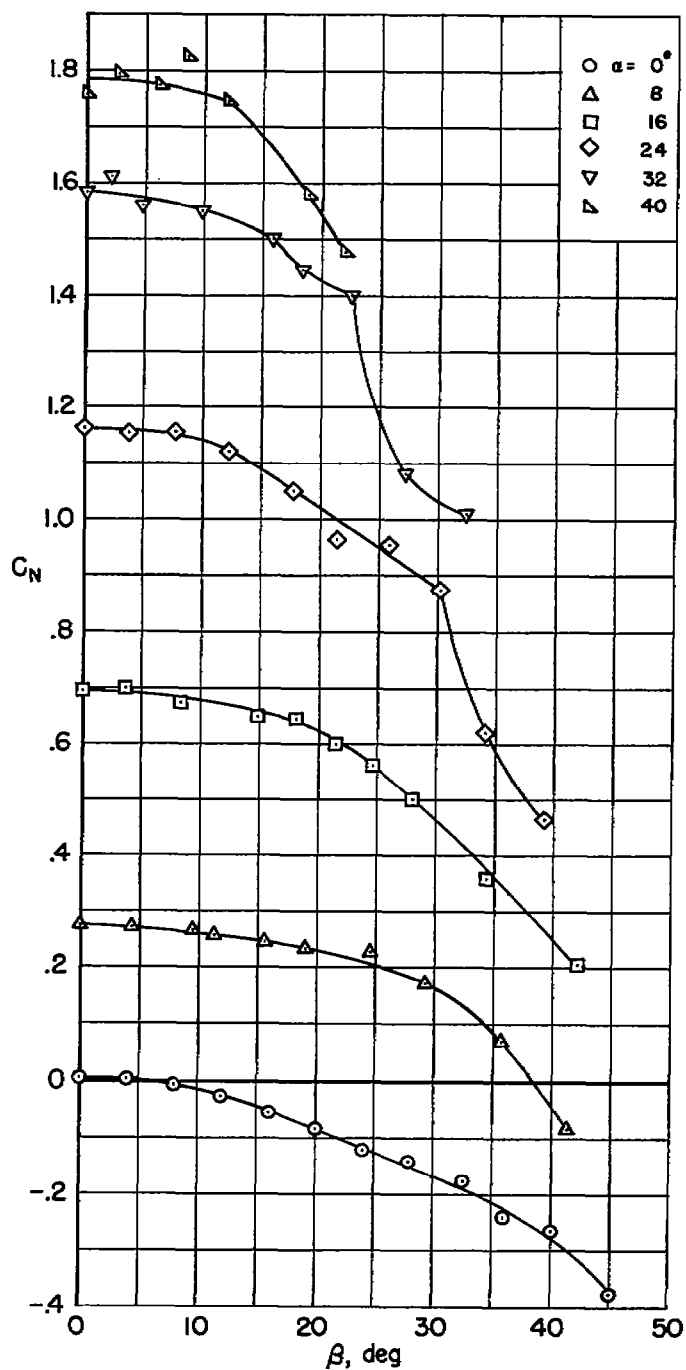
Figure 6.- Continued.

(d) Normal-force coefficient versus sideslip angle.
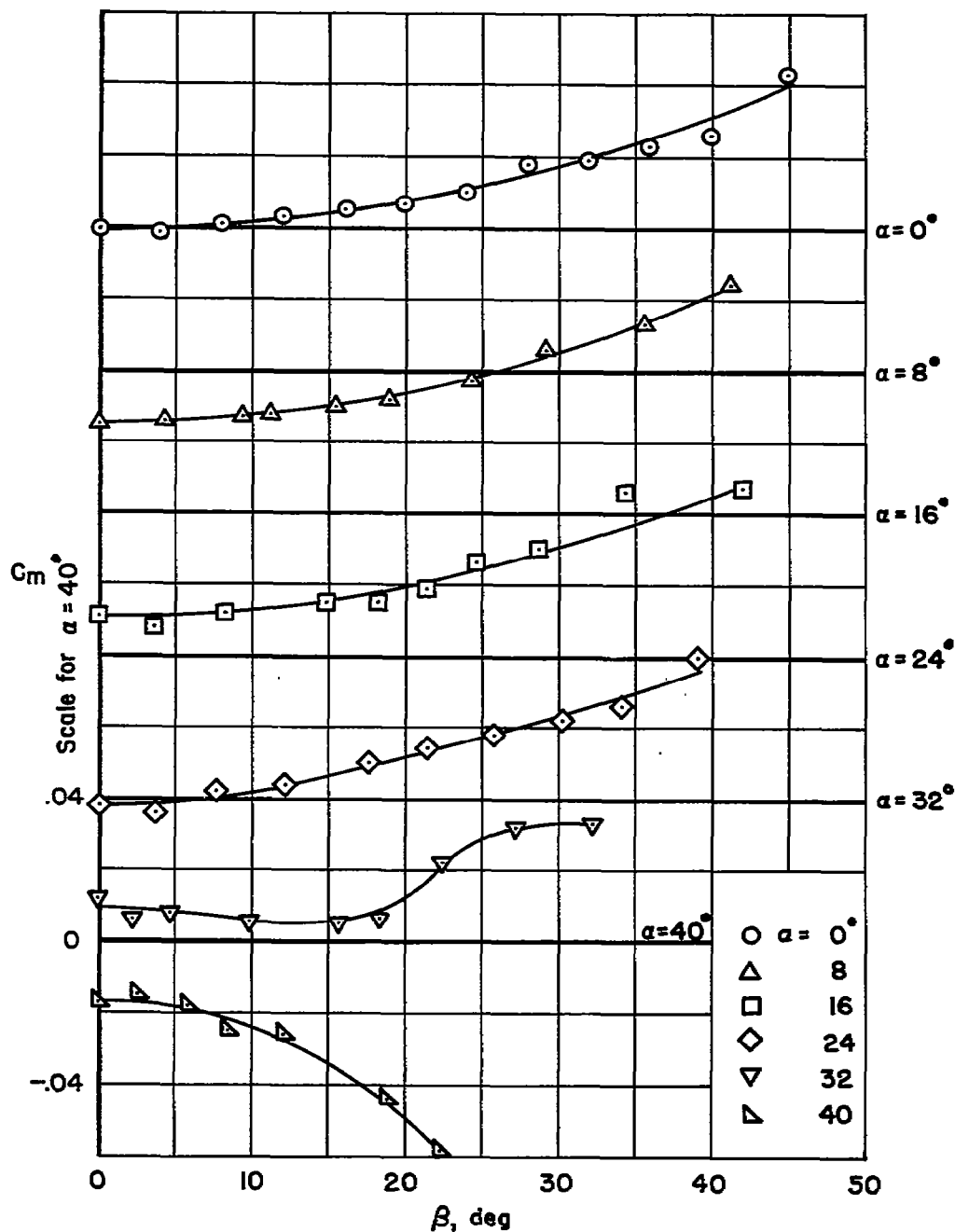
Figure 6.- Continued.

(e) Pitching-moment coefficient versus sideslip angle.

Figure 6.- Continued.
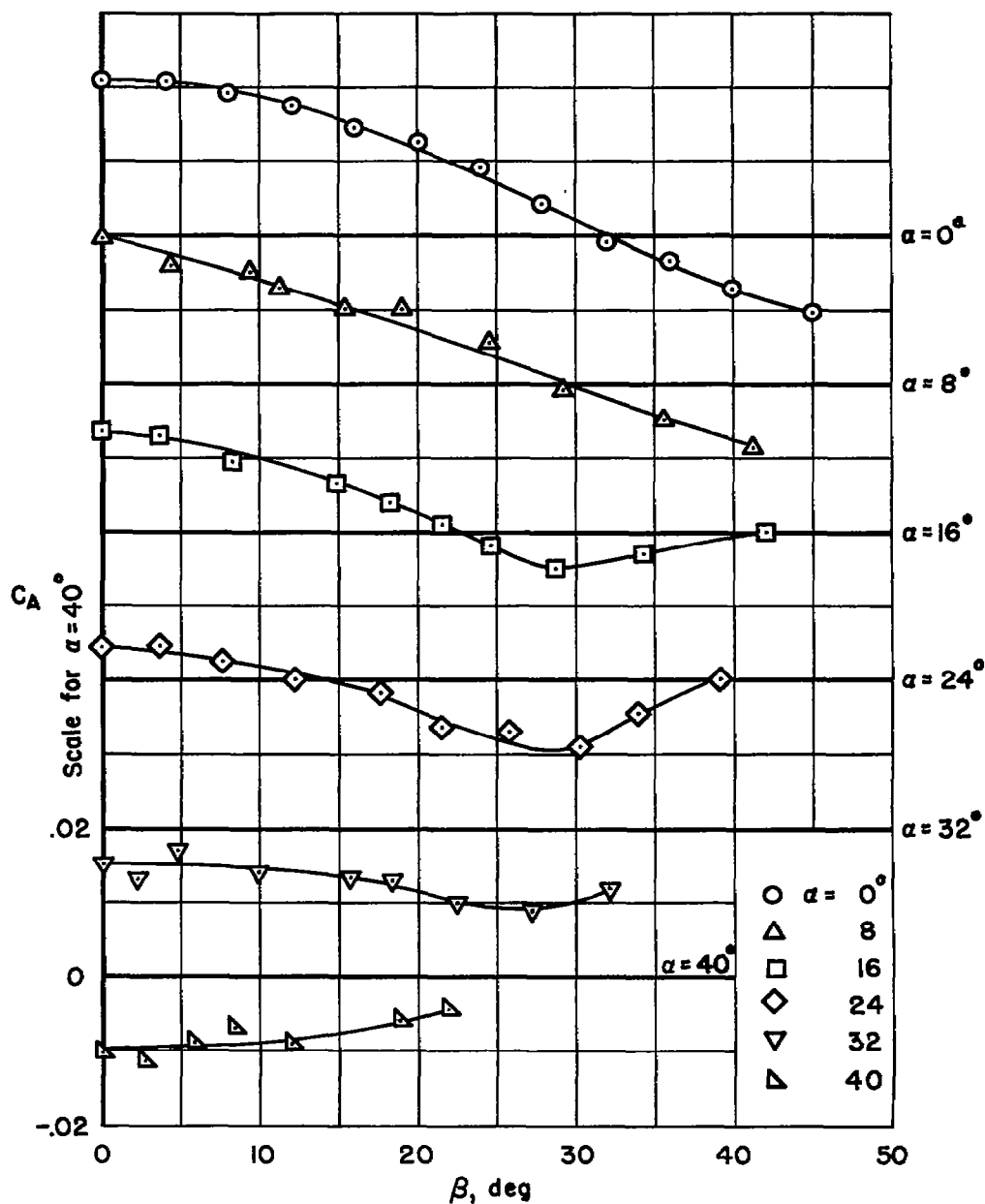
(f) Axial-force coefficient versus sideslip angle.

Figure 6.- Concluded.
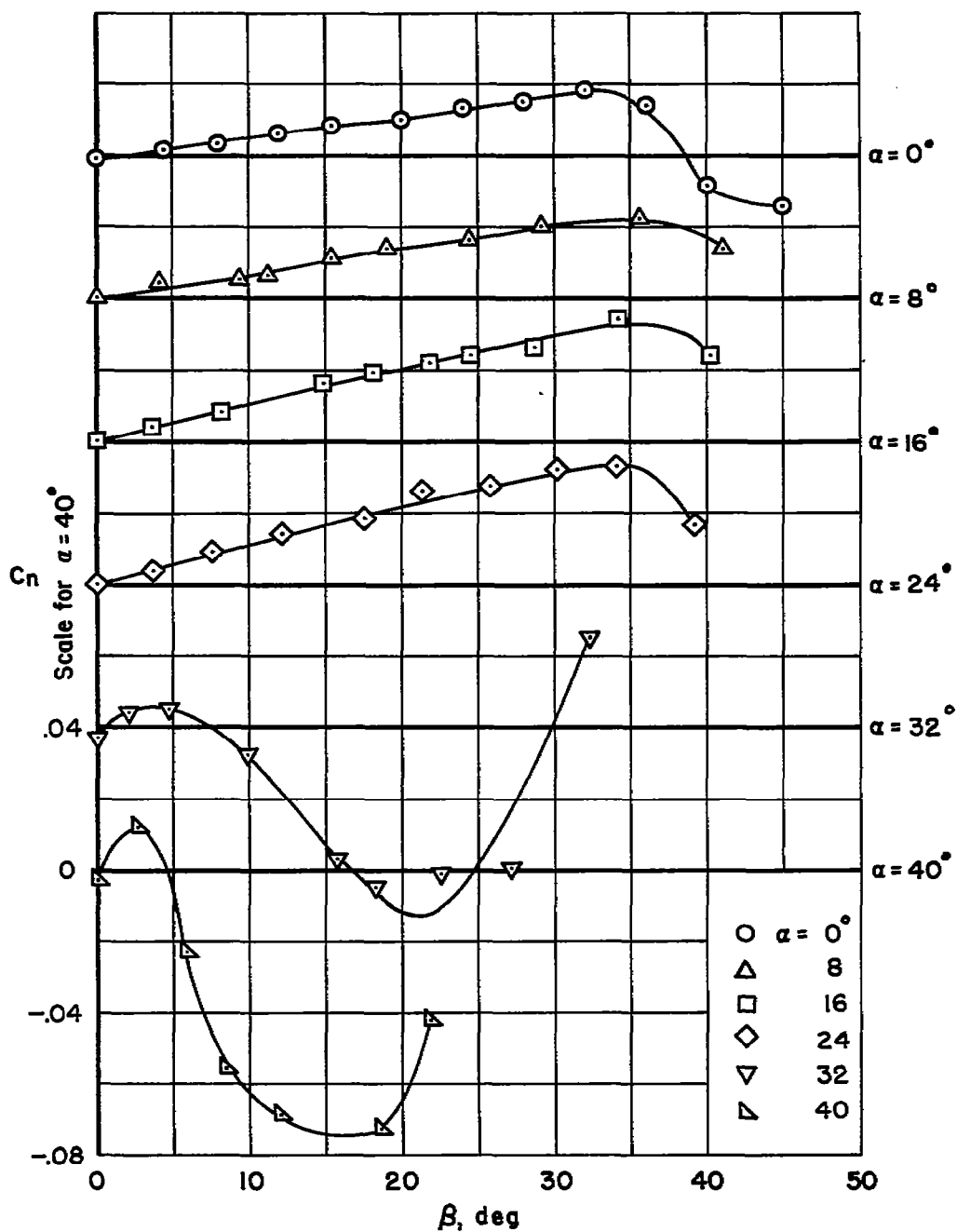
(a) Yawing-moment coefficient versus sideslip angle.

Figure 7.- Force and moment coefficients in sideslip for several angles
of attack; $\Gamma = 0°$, small vertical fin.
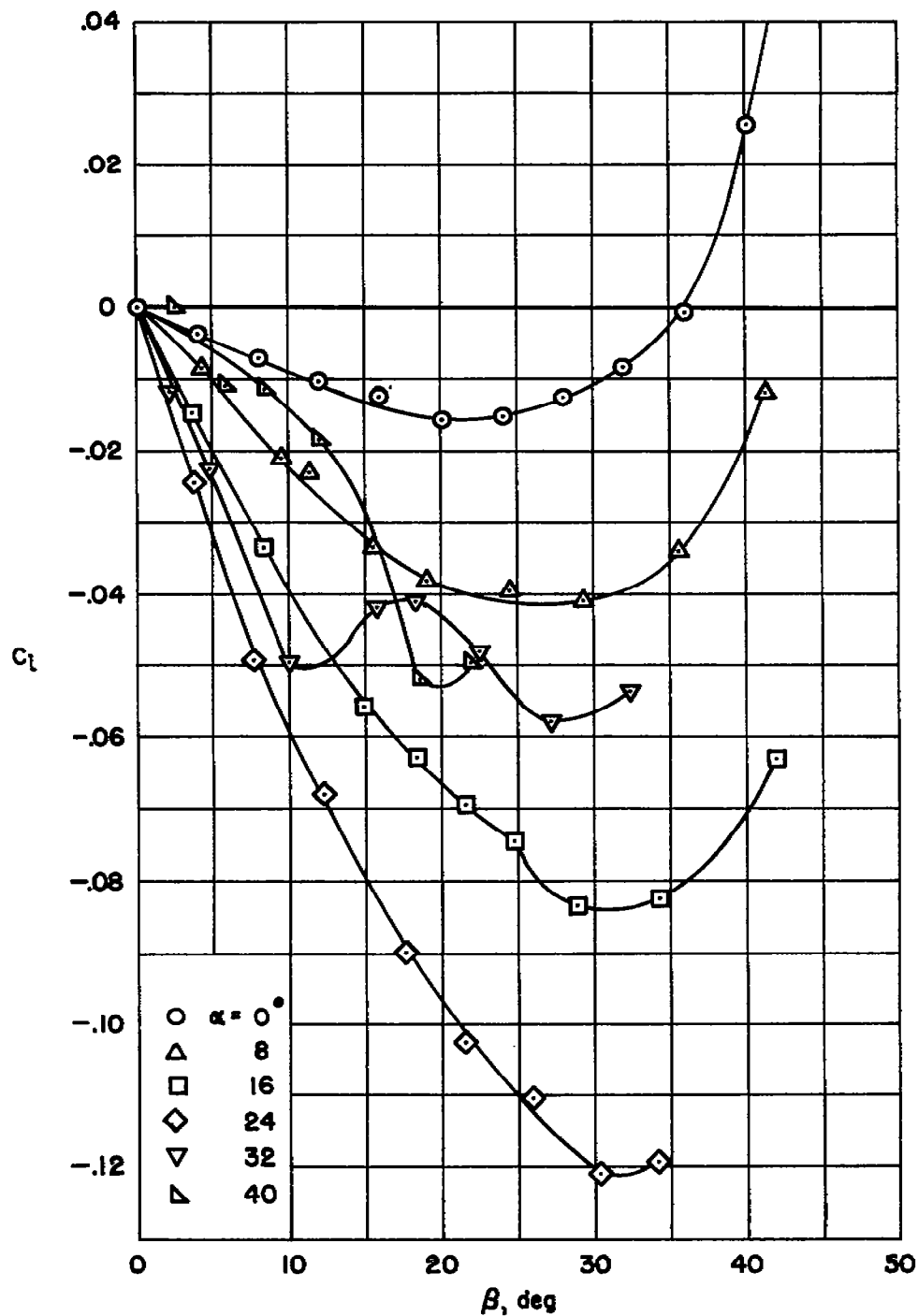
(b) Rolling-moment coefficient versus sideslip angle.

Figure 7.- Continued.

(c) Side-force coefficient versus sideslip angle.
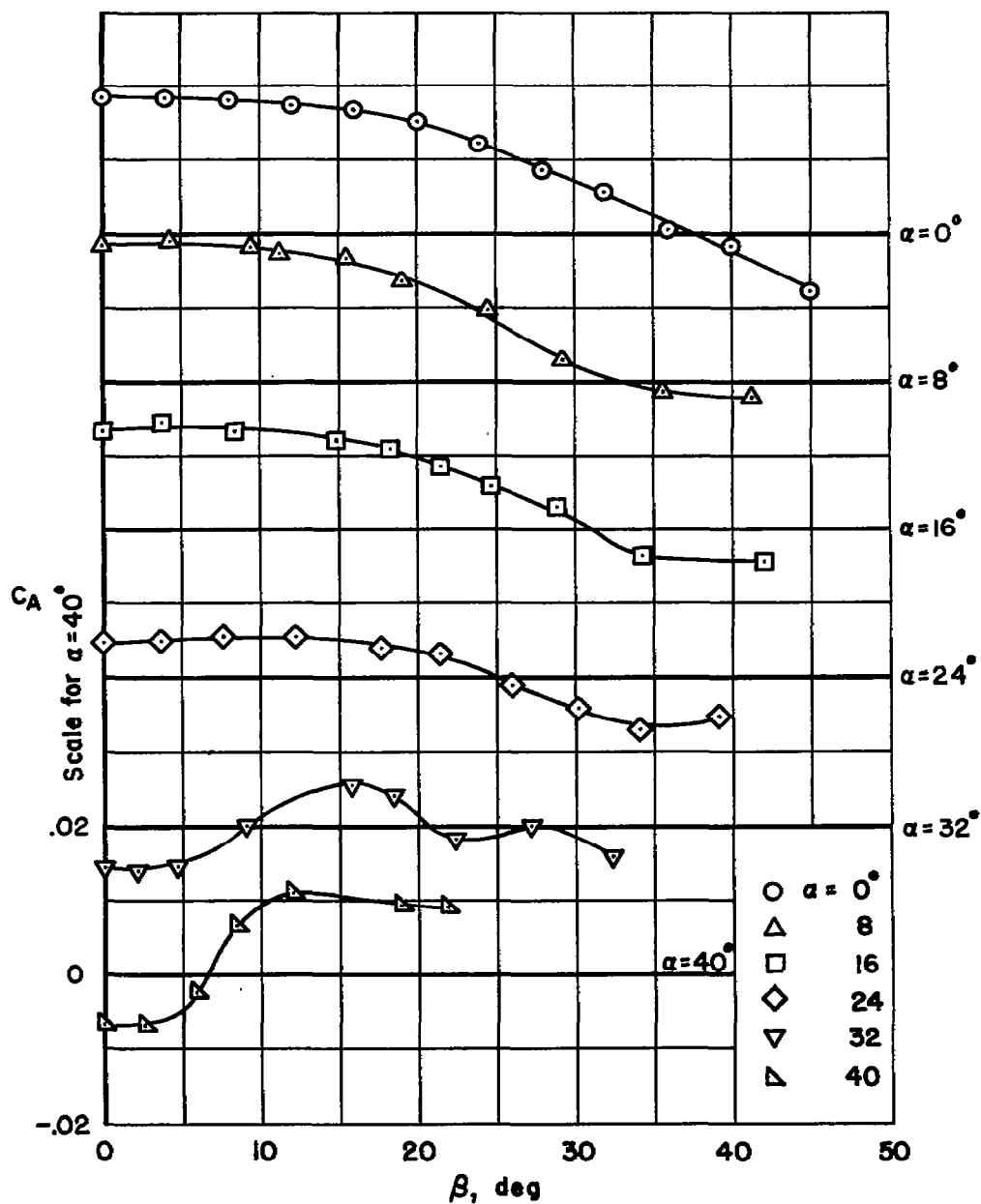
Figure 7.- Continued.

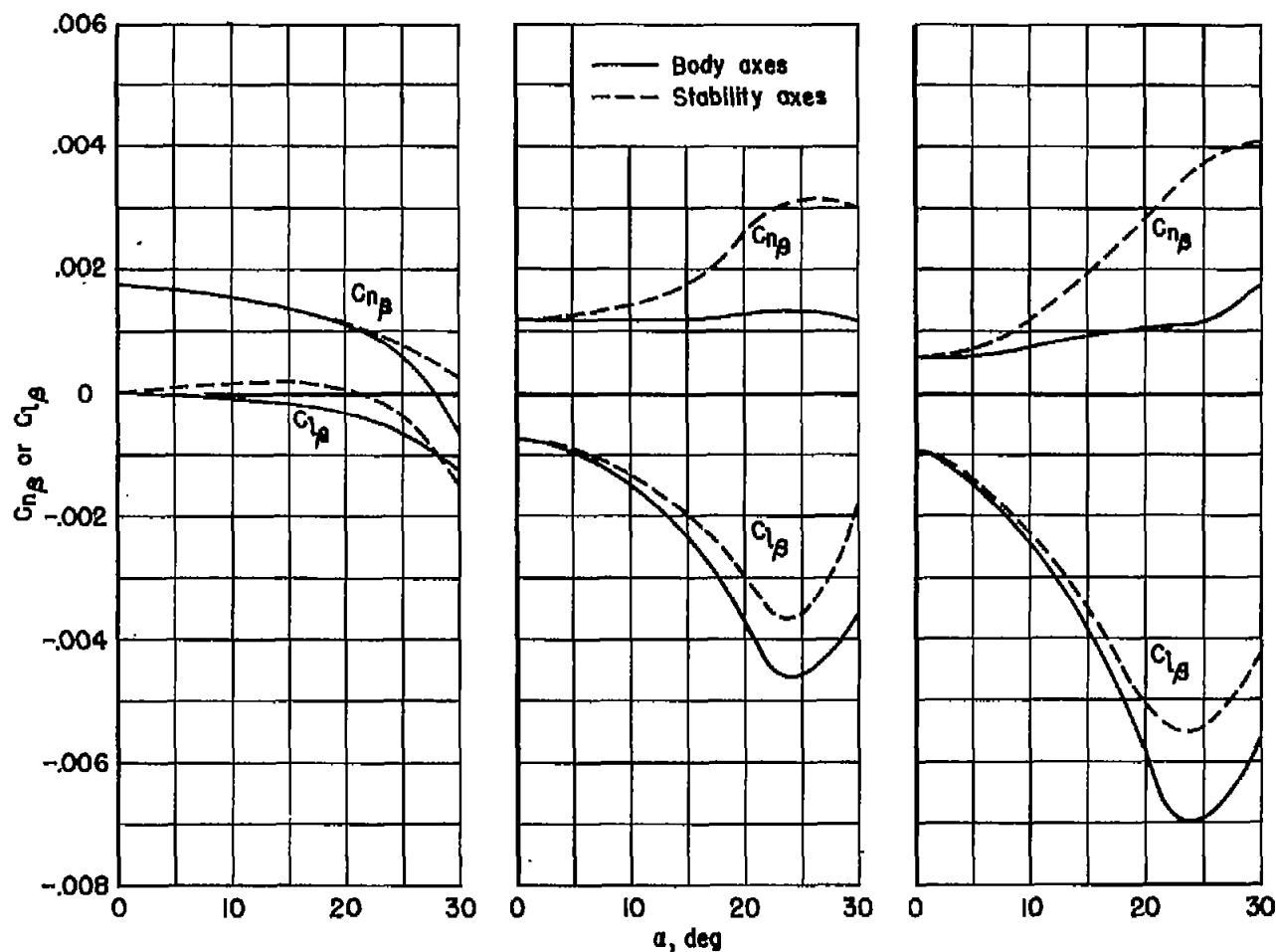(d) Normal-force coefficient versus sideslip angle.

Figure 7.- Continued.

(e) Pitching-moment coefficient versus sideslip angle.

Figure 7.- Continued.

(f) Axial-force coefficient versus sideslip angle.

Figure 7.- Concluded.

(a) $\Gamma = -30°$; large vertical fin.

(b) $\Gamma = -15°$; large vertical fin.

(c) $\Gamma = 0°$; small vertical fin.

Figure 8.- Variation of C_{n_β} and C_{l_β} with angle of attack.